







**Anharmonic host-lattice dynamics enable fast ion conduction in superionic AgI**

Thomas M. Brenner <sup>1</sup>, Christian Gehrman <sup>2</sup>, Roman Korobko <sup>1</sup>, Tsachi Livneh <sup>3</sup>,  
David A. Egger <sup>2,\*</sup> and Omer Yaffe <sup>1,†</sup>

<sup>1</sup>*Department of Materials and Interfaces, Weizmann Institute of Science, Rehovoth 76100, Israel*

<sup>2</sup>*Department of Physics, Technical University of Munich, 85748 Garching, Germany*

<sup>3</sup>*Department of Physics, Nuclear Research Center Negev, P.O. Box 9001, Beer Sheva 84190, Israel*



(Received 18 November 2019; accepted 27 October 2020; published 30 November 2020)

A basic understanding of the driving forces of ion conduction in solids is critical to the development of new solid-state ion conductors. The physical understanding of ion conduction is limited due to strong deviations from harmonic vibrational dynamics in these systems that are difficult to characterize experimentally and theoretically. We overcome this challenge in superionic AgI by combining THz-frequency Raman polarization-orientation measurements and *ab initio* molecular dynamics computations. Our findings demonstrate clear signatures of strong coupling between the mobile ions and host lattice that are of importance to the diffusion process. We first derive a dynamic structural model from the Raman measurements that captures the simultaneous crystal-like and fluidlike properties of this fast ion conductor. Then we show and discuss the importance of anharmonic relaxational motion that arises from the iodine host lattice by demonstrating its strong impact on ion conduction in superionic AgI.

DOI: [10.1103/PhysRevMaterials.4.115402](https://doi.org/10.1103/PhysRevMaterials.4.115402)

Solid-state ion conductors (SSICs) are promising materials for replacing liquid ion conductors used in many important technological applications such as batteries, fuel cells, and supercapacitors, because they are typically nonflammable and could enable higher energy densities [1]. Long-range ionic diffusion in SSICs occurs via thermally activated site-to-site hopping of mobile ions in a host lattice of nondiffusing ions [Fig. 1(a)]. Hopping occurs when mobile ions obtain sufficient thermal energy to overcome migration barriers in the potential energy surface. In traditional ionic transport models, the hopping frequency of the mobile ion is estimated using a harmonic phonon description or included phenomenologically [2–7]. Therefore, these models cannot capture the effects that arise when the mobile ion enters the saddle point region between sites, an intrinsically anharmonic part of the potential energy surface [Fig. 1(a)] [2,3,5,7]. In this region, the motion of the mobile ion may become coupled to other vibrations in the material, changing the potential energy surface of the mobile ion, and potentially modifying the migration barrier [2]. Accurately describing the atomic motions in SSICs therefore requires a departure from the harmonic phonon model of solids [2,3,5,8,9]. Some anharmonic effects, such as coordinated hopping [10,11] and the breakdown of acoustic modes [8,9], have been detected. However, anharmonic coupling of the mobile ion to the host lattice is an overlooked mechanism that may significantly influence ionic conductivity.

Recent computational and experimental work does indeed indicate that the host lattice impacts the ionic conductivity of SSICs in ways not yet captured by traditional

theories [12–22]. Correlations established between ionic conductivity and the physical characteristics of the host lattice, such as mechanical softness, indicate important unexplored coupling mechanisms [12–15]. Specific coupling effects, such as chemical bond frustration [16–18] and the “paddle-wheel” mechanism [20–24] have been proposed with evidence for the latter effect recently detected in state-of-the-art Na<sup>+</sup> and Li<sup>+</sup> conductors [21,22].

Major experimental and theoretical challenges hinder the direct observation and identification of anharmonic effects arising from the host lattice. The direct detection of these coupling effects requires a probe of finite-temperature structural dynamics, rather than a static structural analysis [8,9,16,17,20–22]. From the theoretical side, sophisticated analyses of molecular dynamics computations are required to detect host lattice/mobile ion interactions [16,17,19–22,25]. Experimental investigations of vibrational dynamics in SSICs must contend with the dynamic structural disorder that originates from the hopping of mobile ions among partially populated sites [Fig. 1(b), inset]. In fast ion conducting SSICs, this can result in the breakdown of the phonon quasiparticle picture [8,9], manifesting as broad features in their vibrational spectra. These spectra are difficult to interpret because there is no analytical foundation describing the spectral properties of systems with dynamically broken translational symmetry [8,26–29]. Therefore, a full interpretation of the vibrational spectrum of even  $\alpha$ -AgI, the best-understood and longest-studied superionic SSIC, still remains unresolved [26–31]. Overcoming these issues to provide a detailed account of vibrational coupling between the mobile ions and the host lattice is anticipated to provide useful insights into the role of significant anharmonicities in SSICs.

In this paper, we demonstrate an approach to overcoming these challenges in  $\alpha$ -AgI. We employ Raman

\*david.egger@tum.de

†omer.yaffe@weizmann.ac.il

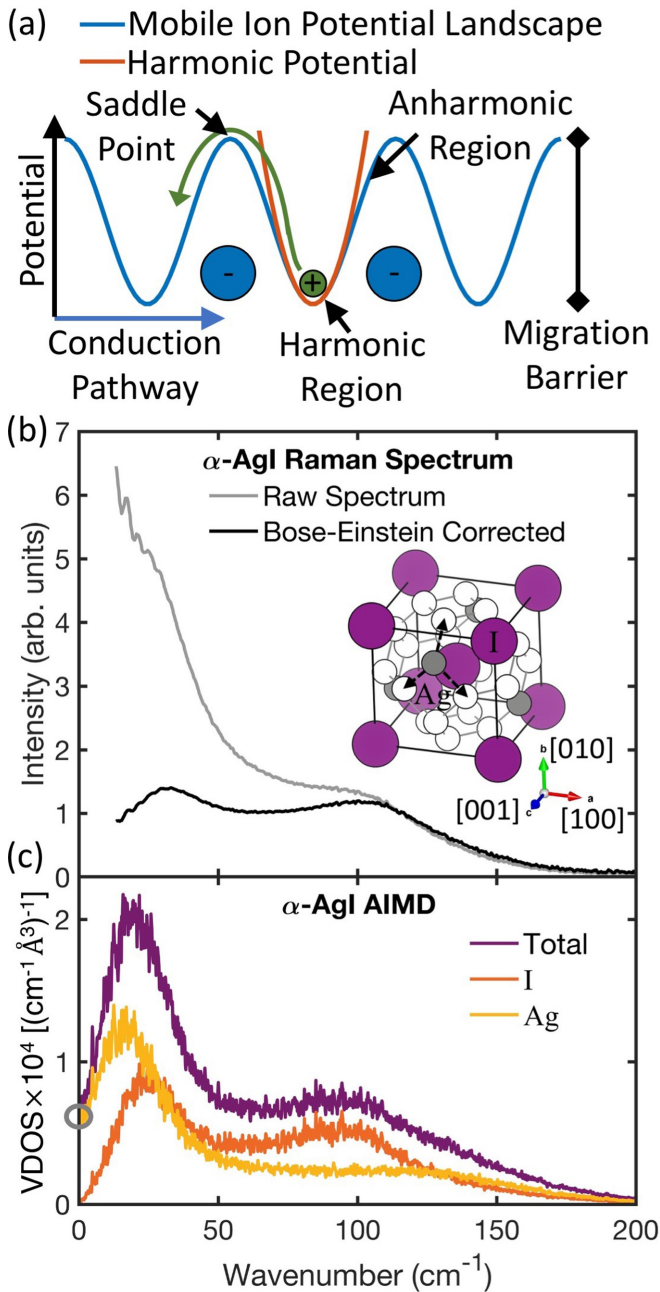


FIG. 1. (a) Conventional ion transport mechanism: A mobile ion (green circle) hops (green arrow) across barriers in the potential landscape due to the host lattice (blue circles) and surrounding mobile ions. (b)  $\alpha$ -AgI Raman spectrum at 443 K. Inset:  $\alpha$ -AgI crystal structure, with I atoms (purple) located at the bcc positions and Ag atoms (dark gray) hopping (black dashed arrows) between empty tetrahedral sites (white). (c) Vibrational density of states (VDOS) of  $\alpha$ -AgI calculated from AIMD at 500 K. The VDOS is decomposed into contributions from each atomic species. The gray circle on the y axis marks the zero-frequency finite VDOS from which a diffusion coefficient of  $3.1 \times 10^{-5} \text{ cm}^2/\text{s}$  was calculated.

polarization-orientation (PO) measurements to reveal unexpected signatures of order in the vibrational dynamics of  $\alpha$ -AgI. This finding enables the development of a microscopic description of the vibrational properties of this SSIC

in terms of localized, coupled motion of Ag and I. Our Raman measurements also reveal the presence of strongly anharmonic, relaxational atomic motions. Through *ab initio* molecular dynamics (AIMD) computations, we show that these relaxational motions involve the iodine host lattice and are coupled to  $\text{Ag}^+$  diffusion. This discovery signifies that anharmonicity plays an important role in the functional properties of this material.

$\alpha$ -AgI exists at ambient pressure between 420 and 831 K.  $\alpha$ -AgI has a cubic structure with the time-average space group  $Im\bar{3}m$ , where I atoms occupy bcc lattice sites and Ag atoms occupy interstitial tetrahedral sites [Fig. 1(b), inset] [32–38]. There are six tetrahedral sites available per Ag atom, and the  $\text{Ag}^+$  dynamically hop between these sites giving rise to the observed ion conductivity. Since all  $\text{Ag}^+$  participate in hopping and have a mean residence time of just 2–3 ps [5,37,39,40], hopping breaks the translational order of the Ag sublattice to below the unit cell level.

In materials with broken translational symmetry, optical vibrations are localized and lack well-defined wave vectors [41]. Consequently, the Raman spectrum of such a material is expected to have contributions from all modes, reflecting the vibrational density of states (VDOS) when corrected for the Bose-Einstein (BE) population factor [41]. The VDOS of  $\alpha$ -AgI can be calculated from AIMD [see methods in the Supplemental Material (SM) [42–45]], since it is accurate in capturing the  $\text{Ag}^+$  diffusion coefficient [46] from the zero-frequency VDOS [gray circle, Fig. 1(c)] [47]. Indeed, the BE-corrected Raman spectrum [Fig. 1(b)] does reflect the AIMD-computed VDOS [Fig. 1(c)], with both showing very broad features near 40 and 100  $\text{cm}^{-1}$ . This observation is consistent with prior interpretations of the  $\alpha$ -AgI Raman spectrum, which have primarily ascribed the spectrum to disorder-induced scattering or a liquidlike scattering response [28–31,48–53].

We now contrast the disorder-induced scattering picture with measurements from a method typically employed to characterize fully crystalline samples: PO Raman (Fig. 2). In the PO method, the Raman spectrum of a single crystal is excited with polarized light whose orientation is rotated stepwise through  $360^\circ$  in the plane of the probed crystal face. The resulting spectral response is filtered for polarizations parallel and perpendicular to the excitation (see methods in SM [42]) [54]. This method probes the components of the Raman polarizability tensor, from which mode symmetries and consequently a structural model can be derived [54,55]. Figure 2(a) shows intensity maps of the PO Raman response of an  $\alpha$ -AgI single crystal (preparation described in SM [42,56,57]) for the parallel and perpendicular configurations at 443 K. Additional measurements covering the stability range of  $\alpha$ -AgI (583 and 723 K) are presented in Fig. S1 [42]. Remarkably, all of the Raman spectral features are found to exhibit clear periodicities in intensity as a function of orientation in both polarization configurations, which establishes specific symmetries for these vibrational features. This apparent crystal-like order in  $\alpha$ -AgI, despite its broken translational symmetry, is unique, since other materials with broken translational symmetry, such as liquids or amorphous solids, cannot show any modulation of intensity with orientation angle (Fig. S2 [42]).

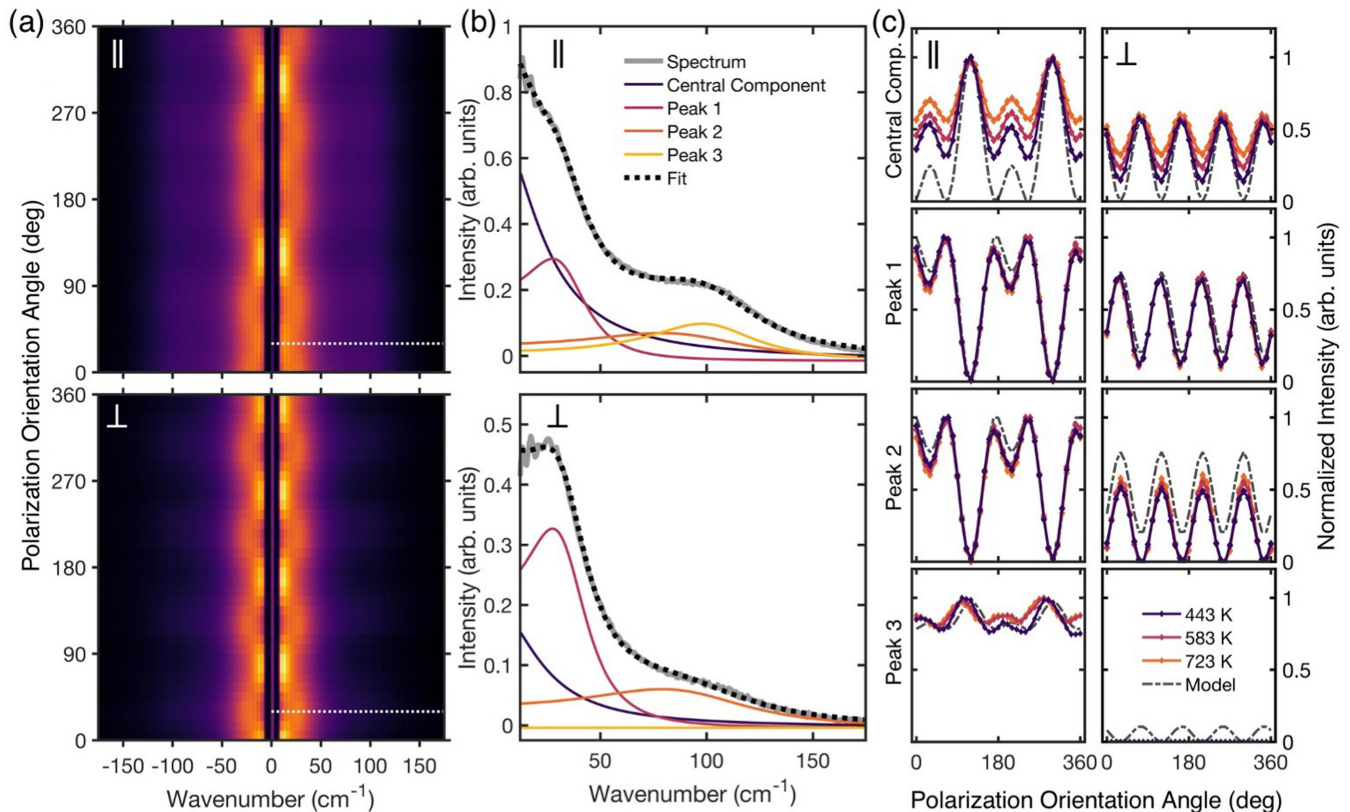


FIG. 2. PO Raman measurements of  $\alpha$ -AgI. (a) PO intensity maps of Raman spectra taken at 443 K, at polarization orientation angles of  $0^\circ$ – $360^\circ$  in parallel ( $\parallel$ ) and perpendicular ( $\perp$ ) polarization configurations, including both Stokes and anti-Stokes scattering. The region between  $-10$  and  $10$   $\text{cm}^{-1}$  is cut off by a notch filter. Spikelike features seen near  $10$   $\text{cm}^{-1}$  are due to interference effects from the notch filter. (b) Representative Raman spectra and their fit components and envelope, for both polarization configurations, taken from the dashed lines in (a). (c) Plots of the normalized intensity coefficient vs polarization orientation angle for all four features, for each of the three temperatures measured. The expected response of the “local tetrahedral oscillator” model is also included (gray dashed line).

The discovery of crystal-like periodicities in PO motivates the development of a dynamic structural model for  $\alpha$ -AgI. First, we identified and fitted each feature by employing the symmetry filtering effect of PO Raman (see fit methodology in the SM [42]); see Fig. 2(b) for representative spectra and corresponding fits, and Table S1 [42] for all fit parameters. The fitting process revealed the characteristic PO intensity response for each Raman feature [Fig. 2(c)], uncovering the four fundamental features of the  $\alpha$ -AgI vibrational spectrum: one central component (fit by a Debye relaxor [58–60]) and three broad peaks (fit by damped Lorentz oscillators [61]) encompassing three distinct symmetries.

A conventional Raman analysis fails to explain the observations in Fig. 2: On the one hand, ascribing the Raman scattering to purely disorder-induced scattering as discussed above cannot explain the crystallinelike symmetries observed. On the other hand, a standard crystal symmetry analysis [62] of the time-average  $Im\bar{3}m$  structure predicts only two Raman-active features of two distinct symmetries (Tables S2 and S3 [42]). Moreover, if we consider only the host lattice, we find that the bcc structure has no Raman activity. Therefore, neither method can capture the symmetry of the real-time structure detected in the PO Raman measurement, which evidently involves the coordinated motion of both Ag and I.

To reconcile this issue, we propose a “local tetrahedral oscillator” model of vibrations that straddles the boundary between crystalline and disordered materials. This model is motivated by the fact that since the disorder in the  $\text{Ag}^+$  ions exists even below the unit cell level, optical vibrations must be localized to tetrahedral configurations of subunit cell size. The critical innovation of our model is that the symmetry observed in the PO response is established locally rather than through the long-range order of a phonon model of vibrations. In our model, when an  $\text{Ag}^+$  hops to a tetrahedral site of the bcc lattice, a transient, orientationally ordered [63], local  $\text{AgI}_4$  tetrahedral oscillator forms [Fig. 3(a)] whose symmetry is probed by our PO Raman measurements (model details in SM, Table S3, and Fig. S3 [42]). This model predicts the number of Raman features we have observed in  $\alpha$ -AgI, their symmetry, and their PO response [Fig. 2(c), dashed line], and therefore provides a comprehensive picture of the vibrational dynamics in  $\alpha$ -AgI.

The agreement of the local tetrahedral oscillator model with the experimental data at all temperatures as shown in Fig. 2(c) is also noteworthy. This agreement indicates that order within the local oscillator is preserved up to 723 K. This is in contrast to prior works that have suggested a transition to completely fluidlike  $\text{Ag}^+$  cations near 700 K



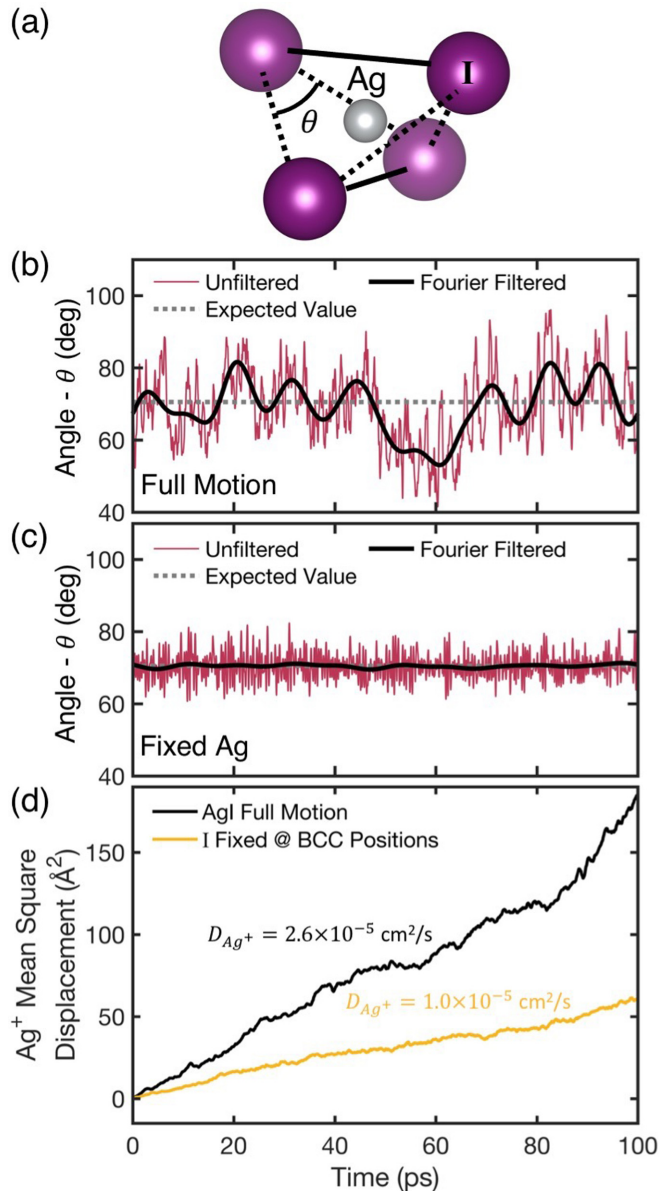


FIG. 3. (a) Diagram of the  $\text{AgI}_4$  tetrahedral site of the bcc lattice, with the I-I-I bond angle  $\theta$  analyzed in AIMD simulations indicated. Lines of the same texture have the same length. (b) Time series of  $\theta$  for  $\alpha$ -AgI AIMD simulation at 500 K with all atomic motions allowed and (c) when  $\text{Ag}^+$  is fixed to zero velocity at tetrahedral sites. (d) Mean-square displacement as a function of time for  $\text{Ag}^+$ , and calculated diffusion coefficient  $D_{\text{Ag}^+}$ , for the following cases: All atomic motions allowed (black line), and I fixed at bcc lattice positions (yellow).

[49–51,64]. However, because our model is localized to a single tetrahedral structure, it cannot rule out a loss of partial order on the scale of several unit cells, as proposed in other works [48,52,53].

The most interesting feature identified from the PO Raman response is the central component (Fig. 2), which is a categorical sign of anharmonic motion. A central component is a manifestation of relaxational motion (i.e., motion that has no restoring force) in the frequency domain, characterized

by a peak centered at zero frequency with a width that is determined by the characteristic relaxation time. The central component we have observed has a width of  $\sim 25 \text{ cm}^{-1}$  (Table S1 [42]) corresponding to a relaxation time of  $\sim 200 \text{ fs}$ . This is much faster than the polarizability changes directly due to ion hopping (2–3 ps relaxation time; see Fig. S4 [42]) [5,39,65–67], but similar to the timescale of relaxation in fluids (Fig. S5 [42]) [68–72]. Our results provide further information on the origins and significance of this feature [39,67]

Our quantification of the PO response of this broad central component [Fig. 2(c)] reveals that it is actually composed of two elements (Fig. S6 [42]), one that is orientation dependent (OD), and one that is orientation independent (OI). Because they have differing PO behavior, these elements must correspond to relaxational motions of differing physical origin.

The PO response of the OI element is distinctly “liquid-like.” As in a fluid, this element has no orientation dependence and is depolarized since it has a high ratio of perpendicular to parallel intensity (compare to the central component of Fig. S2 [42]). The OI element is the only Raman feature with an appreciable temperature dependence. It grows in prominence with increasing temperature in both parallel and perpendicular configurations [Fig. 2(c), and Fig. S6 [42]], but remains fully reversible and does not indicate, for instance, sample degradation effects. The increasing dominance of this element with increasing temperature suggests a continuous change toward a more fluidlike condition throughout the stability region of the  $\alpha$  phase. This component may potentially be associated with the proposed loss of  $\text{Ag}^+$  partial order discussed above [48,52,53].

The OD element of the central component is identified by its symmetry as one of the fundamental modes of the local tetrahedral oscillator model (Fig. S6, Table S3 [42]). If the system was fully harmonic, this element would present as a normal mode of finite frequency, typically the lowest-frequency mode in a tetrahedral molecule according to its symmetry [73]. However, our PO Raman measurements have clearly established that the atomic motions involved are relaxational in nature. To explain this, we hypothesize that the OD element of the central component arises from overdamping of this vibrational mode of the local tetrahedral oscillator through anharmonic coupling to  $\text{Ag}^+$  hopping. The very high hopping rate of  $\text{Ag}^+$  prevents this mode from completing even a single period.

Stimulated by these observations, we investigate via AIMD the relationship between iodine relaxational motion and  $\text{Ag}^+$  diffusion. Our approach is to temporally and spatially resolve atomic motions in the  $\text{AgI}_4$  tetrahedra of the local tetrahedral oscillator model. Specifically, we investigate dynamically changing tetrahedral geometries by computing trajectories of the I-I-I bond angle  $\theta$  [Fig. 3(a)] in one selected  $\text{AgI}_4$  tetrahedron. Any deviations of this bond angle from its expected value, i.e., the  $70.5^\circ$  angle of the bcc lattice, indicate distortions to the shape of the tetrahedron. The red curve of Fig. 3(b) shows an AIMD trajectory of  $\theta$ , which displays very large angular fluctuations that appear on shorter but also longer timescales (e.g., see the long-lived deviation at  $\sim 60 \text{ ps}$ ). As discussed above, the most interesting aspect of the local tetrahedral oscillator model was the low-frequency relaxational motion giving rise to the central component in the PO Raman

response. To probe the atomic motions associated with it, we obtained trajectories of  $\theta$  [black curve, Fig. 3(b)] retaining only the low-frequency ( $<5 \text{ cm}^{-1}$ ) dynamics (see SM for further details [42]). This frequency regime exclusively contains relaxational components that are not present in purely harmonic systems. Figure 3(b) demonstrates that in the low-frequency regime  $\theta$  undergoes fluctuations of up to  $15^\circ$  from its expectation value, over a period of up to 10 ps, indicating large, long-lived rearrangements of the iodine tetrahedron that arise from anharmonic relaxation events. Although we cannot exclude that yet another relaxational motion within the material is actually causing the central component observed in Raman scattering, both experiment and theory indicate anharmonic relaxational motion in the iodine host lattice.

A pair of AIMD-enabled gedanken experiments establishes the coupling between the iodine host lattice and  $\text{Ag}^+$  motion. First, stipulating  $\text{Ag}^+$  to be fixed with zero velocity at tetrahedral sites, we find that the large amplitude oscillations of  $\theta$  at low frequency disappear [black curve, Fig. 3(c)]. This indicates that  $\text{Ag}^+$  motion (either vibrational and/or hopping) is causally connected with the relaxational motion of the I lattice. Second, to assess how I motion impacts  $\text{Ag}^+$  diffusion, we consider the mean-squared displacement of  $\text{Ag}^+$  ions versus time [Fig. 3(d)], the slope of which is proportional to the diffusion constant. Importantly, we find that freezing I motion impedes  $\text{Ag}^+$  diffusion, which indicates that the dynamic rearrangement of I is an important factor in ion diffusion, consistent with prior findings [74–76]. Further analysis shows that statically displaced I atoms, simulated at instantaneous configurations obtained as snapshots of the AIMD simulations, also lead to strongly reduced  $\text{Ag}^+$  diffusion (Fig. S7 [42]). These two gedanken experiments establish the strong interconnections between anharmonic relaxational I host-lattice motions and the dynamics of  $\text{Ag}^+$ .

We suggest that a broad central component and corresponding relaxational motion of the host lattice may be indicators of a good ion conductor. While a broader survey of materials is needed for confirmation, we do note that several other highly conductive SSICs also show signs of a broad central component in their Raman response [27,39,77]. Conversely, the much less conductive  $\beta$  phase of  $\text{AgI}$  and non-ion-conducting quasiharmonic GaAs do not show a central component (Fig. S5 [42]). The proposed indicator would bring a physical understanding of microscopic dynamics to ionic conductor design that is not available from current empirical indicators [78,79]. Moreover, this indicator explicitly includes information about the requisite nature of the

lattice dynamics that can be tested with currently available tools. The idea that anharmonic host-lattice dynamics are required brings many disparate ideas under one umbrella: Coupling mechanisms such as chemical bond frustration and the “paddle-wheel effect” fall into this category and it is anticipated these mechanisms will show the expected relaxation phenomena.

In conclusion, using PO Raman measurements and AIMD calculations, we developed an improved understanding of the vibrational dynamics of the archetypal solid-state ion conductor  $\alpha\text{-AgI}$ . We introduced the local tetrahedral oscillator model in which the  $\alpha\text{-AgI}$  vibrational dynamics are localized to an  $\text{AgI}_4$  tetrahedral configuration. The success of our model demonstrates the value of a local picture of vibrational dynamics in materials with dynamic structural disorder. Within that picture we have identified the presence of anharmonic relaxational motion in our Raman measurements and the AIMD simulations, which demonstrated an anharmonic relaxational component in the iodine host lattice. Our AIMD computations indicate that iodine relaxation is causally connected to  $\text{Ag}^+$  motion, and vice versa  $\text{Ag}^+$  diffusion is strongly impacted by iodine vibrations. These results show that anharmonic motion of the host lattice is a critical component of the ion transport process in  $\alpha\text{-AgI}$ . We hope our findings revitalize the efforts to understand the deep connection between vibrational dynamics and ionic conductivity, and thereby may lead to new SSIC design principles.

We would like to thank Ishay Feldman (WIS) for performing x-ray diffraction measurements, Lior Segev (WIS) for critical software development, and Claudio Cazorla (UNSW Sydney) and Brandon C. Wood (LLNL) for fruitful discussions. O.Y. acknowledges funding from the following: the Benozio Endowment Fund, the Ilse Katz Institute, the Henry Chanoch Kreter Institute, the Soref New Scientists Start Up Fund, Carolito Stiftung, the Abraham and Sonia Rochlin Foundation, and Erica A. Drake and Robert Drake. D.A.E. acknowledges funding from the following: the Alexander von Humboldt Foundation within the framework of the Sofja Kovalevskaja Award, endowed by the German Federal Ministry of Education and Research; the Technical University of Munich - Institute for Advanced Study, funded by the German Excellence Initiative and the European Union Seventh Framework Programme under Grant Agreement No. 291763; and the Deutsche Forschungsgemeinschaft (DFG, German Research Foundation) under Germany’s Excellence Strategy - EXC 2089/1–390776260.

[1] A. Manthiram, X. Yu, and S. Wang, *Nat. Rev. Mater.* **2**, 16103 (2017).  
 [2] S. A. Rice, *Phys. Rev.* **112**, 804 (1958).  
 [3] G. H. Vineyard, *J. Phys. Chem. Solids* **3**, 121 (1957).  
 [4] D. P. Almond and A. R. West, *Solid State Ionics* **23**, 27 (1987).  
 [5] *Physics of Superionic Conductors*, edited by M. B. Salamon (Springer, Berlin, 1979).  
 [6] R. A. Huggins, *Advanced Batteries* (Springer, New York, 2009).  
 [7] J. Maier, *Physical Chemistry of Ionic Materials: Ions and Electrons in Solids*, 1st ed. (Wiley, Hoboken, NJ, 2004).

[8] J. L. Niedziela, D. Bansal, A. F. May, J. Ding, T. Lanigan-Atkins, G. Ehlers, D. L. Abernathy, A. Said, and O. Delaire, *Nat. Phys.* **15**, 73 (2019).  
 [9] J. Ding, J. L. Niedziela, D. Bansal, J. Wang, X. He, A. F. May, G. Ehlers, D. L. Abernathy, A. Said, A. Alatas, Y. Ren, G. Arya, and O. Delaire, *Proc. Natl. Acad. Sci. U.S.A.* **117**, 3930 (2020).  
 [10] X. He, Y. Zhu, and Y. Mo, *Nat. Commun.* **8**, 15893 (2017).  
 [11] R. J. Cava and D. B. McWhan, *Phys. Rev. Lett.* **45**, 2046 (1980).

- [12] M. A. Kraft, S. P. Culver, M. Calderon, F. Böcher, T. Krauskopf, A. Senyshyn, C. Dietrich, A. Zevalkink, J. Janek, and W. G. Zeier, *J. Am. Chem. Soc.* **139**, 10909 (2017).
- [13] T. Krauskopf, C. Pompe, M. A. Kraft, and W. G. Zeier, *Chem. Mater.* **29**, 8859 (2017).
- [14] T. Krauskopf, S. Muy, S. P. Culver, S. Ohno, O. Delaire, Y. Shao-Horn, and W. G. Zeier, *J. Am. Chem. Soc.* **140**, 14464 (2018).
- [15] S. Muy, J. C. Bachman, L. Giordano, H.-H. Chang, D. L. Abernathy, D. Bansal, O. Delaire, S. Hori, R. Kanno, F. Maglia, S. Lupart, P. Lamp, and Y. Shao-Horn, *Energy Environ. Sci.* **11**, 850 (2018).
- [16] K. E. Kweon, J. B. Varley, P. Shea, N. Adelstein, P. Mehta, T. W. Heo, T. J. Udovic, V. Stavila, and B. C. Wood, *Chem. Mater.* **29**, 9142 (2017).
- [17] N. Adelstein and B. C. Wood, *Chem. Mater.* **28**, 7218 (2016).
- [18] L. Duchêne, S. Lunghammer, T. Burankova, W.-C. Liao, J. P. Embs, C. Copéret, H. M. R. Wilkening, A. Remhof, H. Hagemann, and C. Battaglia, *Chem. Mater.* **31**, 3449 (2019).
- [19] N. J. J. de Klerk and M. Wagemaker, *Chem. Mater.* **28**, 3122 (2016).
- [20] J. G. Smith and D. J. Siegel, *Nat. Commun.* **11**, 1483 (2020).
- [21] Z. Zhang, P.-N. Roy, H. Li, M. Avdeev, and L. F. Nazar, *J. Am. Chem. Soc.* **141**, 19360 (2019).
- [22] Z. Zhang, H. Li, K. Kaup, L. Zhou, P.-N. Roy, and L. F. Nazar, *Matter* **2**, 1667 (2020).
- [23] M. Jansen, *Angew. Chem., Int. Ed. Engl.* **30**, 1547 (1991).
- [24] A. Lundén, *Solid State Commun.* **65**, 1237 (1988).
- [25] A. K. Sagotra, D. Chu, and C. Cazorla, *Phys. Rev. Mater.* **3**, 035405 (2019).
- [26] R. C. Hanson, T. A. Fjeldly, and H. D. Hochheimer, *Phys. Status Solidi B* **70**, 567 (1975).
- [27] D. A. Gallagher and M. V. Klein, *Phys. Rev. B* **19**, 4282 (1979).
- [28] R. Alben and G. Burns, *Phys. Rev. B* **16**, 3746 (1977).
- [29] E. Cazzanelli, A. Fontana, G. Mariotto, V. Mazzacurati, G. Ruocco, and G. Signorelli, *Phys. Rev. B* **28**, 7269 (1983).
- [30] M. J. Delaney and S. Ushioda, *Phys. Rev. B* **16**, 1410 (1977).
- [31] S. Ushioda and M. J. Delaney, Liquid-like Raman scattering by superionic materials, in *Inelastic Light Scattering*, edited by E. Burstein and H. Kawamura (Pergamon, New York, 1980), pp. 67–70.
- [32] R. J. Cava, F. Reidinger, and B. J. Wuensch, *Solid State Commun.* **24**, 411 (1977).
- [33] A. F. Wright and B. E. F. Fender, *J. Phys. C* **10**, 2261 (1977).
- [34] S. Hoshino, T. Sakuma, and Y. Fujii, *Solid State Commun.* **22**, 763 (1977).
- [35] S. Hoshino, *J. Phys. Soc. Jpn.* **12**, 315 (1957).
- [36] M. J. Cooper and M. Sakata, *Acta Crystallogr., Sect. A* **35**, 989 (1979).
- [37] J. B. Boyce, T. M. Hayes, W. Stutius, and J. C. Mikkelsen, *Phys. Rev. Lett.* **38**, 1362 (1977).
- [38] B. C. Wood and N. Marzari, *Phys. Rev. Lett.* **97**, 166401 (2006).
- [39] R. J. Nemanich, R. M. Martin, and J. C. Mikkelsen, Light scattering from correlated ion fluctuations in ionic conductors, in *Inelastic Light Scattering* (Ref. [31]), p. 79.
- [40] K. Funke, *Prog. Solid State Chem.* **11**, 345 (1976).
- [41] R. Shuker and R. W. Gammon, *Phys. Rev. Lett.* **25**, 222 (1970).
- [42] See Supplemental Material at <http://link.aps.org/supplemental/10.1103/PhysRevMaterials.4.115402> for supporting experimental and computational details.
- [43] G. Kresse and J. Furthmüller, *Phys. Rev. B* **54**, 11169 (1996).
- [44] G. Kresse and D. Joubert, *Phys. Rev. B* **59**, 1758 (1999).
- [45] J. P. Perdew, K. Burke, and M. Ernzerhof, *Phys. Rev. Lett.* **77**, 3865 (1996).
- [46] A. Kvist and R. Tärneberg, *Z. Naturforsch., A: Phys. Sci.* **25**, 257 (1970).
- [47] A. Nitzan, *Chemical Dynamics in Condensed Phases: Relaxation, Transfer and Reactions in Condensed Molecular Systems* (Oxford University Press, Oxford, UK, 2006).
- [48] K. O’Sullivan, G. Chiarotti, and P. A. Madden, *Phys. Rev. B* **43**, 13536 (1991).
- [49] G. Mariotto, A. Fontana, E. Cazzanelli, and M. P. Fontana, *Phys. Status Solidi B* **101**, 341 (1980).
- [50] A. Fontana, G. Mariotto, and M. P. Fontana, *Phys. Rev. B* **21**, 1102 (1980).
- [51] G. Mariotto, A. Fontana, E. Cazzanelli, F. Rocca, M. P. Fontana, V. Mazzacurati, and G. Signorelli, *Phys. Rev. B* **23**, 4782 (1981).
- [52] E. Cazzanelli, A. Fontana, G. Mariotto, F. Rocca, V. Mazzacurati, G. Ruocco, and G. Signorelli, *Solid State Ionics* **5**, 473 (1981).
- [53] V. Mazzacurati, G. Ruocco, G. Signorelli, E. Cazzanelli, A. Fontana, and G. Mariotto, *Phys. Rev. B* **26**, 2216 (1982).
- [54] K. Mizoguchi and S. Nakashima, *J. Appl. Phys.* **65**, 2583 (1989).
- [55] W. Hayes and R. Loudon, *Scattering of Light by Crystals* (Dover, New York, 2004).
- [56] L. Helmholtz, *J. Chem. Phys.* **3**, 740 (1935).
- [57] D. R. Mills, C. M. Perrott, and N. H. Fletcher, *J. Cryst. Growth* **6**, 266 (1970).
- [58] O. Yaffe, Y. Guo, L. Z. Tan, D. A. Egger, T. Hull, C. C. Stoumpos, F. Zheng, T. F. Heinz, L. Kronik, M. G. Kanatzidis, J. S. Owen, A. M. Rappe, M. A. Pimenta, and L. E. Brus, *Phys. Rev. Lett.* **118**, 136001 (2017).
- [59] E. Bouziane, M. D. Fontana, and M. Ayadi, *J. Phys.: Condens. Matter* **15**, 1387 (2003).
- [60] M. D. Fontana, H. Idrissi, and K. Wojcik, *Europhys. Lett.* **11**, 419 (1990).
- [61] The extreme width of the peaks observed likely arises from a combination of lifetime and inhomogeneous broadening. The inhomogeneous broadening can arise from the many possible local environments of the local tetrahedral oscillator, among other possible sources. Therefore, while we find the damped Lorentz oscillator is the only physically viable model at these low frequencies (see fit methodology in SM [42]), the peak width likely does not reflect purely a vibrational lifetime.
- [62] D. L. Rousseau, R. P. Bauman, and S. P. S. Porto, *J. Raman Spectrosc.* **10**, 253 (1981).
- [63] “Orientational order” denotes the integer number of tetrahedral ( $D_{2d}$ -symmetry) orientations allowed by the bcc lattice.
- [64] Prior work also attributed a drop in scattering intensity at high temperature to such an order-disorder transition, however, we observed a drop in intensity due to increased diffuse reflectivity from morphological changes at the surface of the sample (see methods in SM [42]).
- [65] T. Geisel, *Solid State Commun.* **24**, 155 (1977).
- [66] W. Dieterich, T. Geisel, and I. Peschel, *Z. Phys. B* **29**, 5 (1978).
- [67] G. Winterling, W. Senn, M. Grimsditch, and R. Katiyar, in *Proceedings of the International Conference on Lattice Dynamics*, edited by M. Balkanski (Flammarion, Paris, 1977).

- [68] J. A. Bucaro and T. A. Litovitz, *J. Chem. Phys.* **55**, 3585 (1971).
- [69] P. A. Fleury, J. M. Worlock, and H. L. Carter, *Phys. Rev. Lett.* **30**, 591 (1973).
- [70] S. Bratos and G. Tarjus, *Phys. Rev. A* **24**, 1591 (1981).
- [71] E. Dayan, J. Loisel, L. Berreby, E. Dervil, and J. P. Pinan-Lucarré, *J. Raman Spectrosc.* **26**, 341 (1995).
- [72] V. Mazzacurati, A. Nucara, M. A. Ricci, G. Ruocco, and G. Signorelli, *J. Chem. Phys.* **93**, 7767 (1990).
- [73] K. Nakamoto, *Infrared and Raman Spectra of Inorganic and Coordination Compounds*, 6th ed. (Wiley, Hoboken, NJ, 2009).
- [74] W. Schommers, *Phys. Rev. Lett.* **38**, 1536 (1977).
- [75] M. Hokazono, A. Ueda, and Y. Hiwatari, *Solid State Ionics* **13**, 151 (1984).
- [76] Y. Yokoyama and M. Kobayashi, *Solid State Ionics* **159**, 79 (2003).
- [77] L. L. Chase, C. H. Hao, and G. D. Mahan, *Solid State Commun.* **18**, 401 (1976).
- [78] J. C. Bachman, S. Muy, A. Grimaud, H.-H. Chang, N. Pour, S. F. Lux, O. Paschos, F. Maglia, S. Lupart, P. Lamp, L. Giordano, and Y. Shao-Horn, *Chem. Rev.* **116**, 140 (2016).
- [79] Y. Wang, W. D. Richards, S. P. Ong, L. J. Miara, J. C. Kim, Y. Mo, and G. Ceder, *Nat. Mater.* **14**, 1026 (2015).